

**$g$ -factor and static quadrupole moment for the wobbling mode in  $^{133}\text{La}$** Q. B. Chen,<sup>1,\*</sup> S. Frauendorf,<sup>2,†</sup> N. Kaiser,<sup>1,‡</sup> Ulf-G. Meißner,<sup>3,4,5,§</sup> and J. Meng<sup>6,7,¶</sup><sup>1</sup>*Physik-Department, Technische Universität München, D-85747 Garching, Germany*<sup>2</sup>*Physics Department, University of Notre Dame, Notre Dame, IN 46556, USA*<sup>3</sup>*Helmholtz-Institut für Strahlen- und Kernphysik and Bethe Center for Theoretical Physics, Universität Bonn, D-53115 Bonn, Germany*<sup>4</sup>*Institute for Advanced Simulation, Institut für Kernphysik and Jülich Center for Hadron Physics, Forschungszentrum Jülich, D-52425 Jülich, Germany*<sup>5</sup>*Ivane Javakhishvili Tbilisi State University, 0186 Tbilisi, Georgia*<sup>6</sup>*State Key Laboratory of Nuclear Physics and Technology, School of Physics, Peking University, Beijing 100871, China*<sup>7</sup>*Yukawa Institute for Theoretical Physics, Kyoto University, Kyoto 606-8502, Japan*

(Dated: June 2, 2020)

The  $g$ -factor and static quadrupole moment for the wobbling mode in the nuclide  $^{133}\text{La}$  are investigated as functions of the spin  $I$  by employing the particle rotor model. The model can reproduce the available experimental data of  $g$ -factor and static quadrupole moment. The properties of the  $g$ -factor and static quadrupole moment as functions of  $I$  are interpreted by analyzing the angular momentum geometry of the collective rotor, proton-particle, and total nuclear system. It is demonstrated that the experimental value of the  $g$ -factor at the bandhead of the yrast band leads to the conclusion that the rotor angular momentum is  $R \simeq 2$ . Furthermore, the variation of the  $g$ -factor with the spin  $I$  yields the information that the angular momenta of the proton-particle and total nuclear system are oriented parallel to each other. The negative values of the static quadrupole moment over the entire spin region are caused by an alignment of the total angular momentum mainly along the short axis. Static quadrupole moment differences between the wobbling and yrast band originate from a wobbling excitation with respect to the short axis.

The collective motions of a triaxially deformed nucleus, that is shaped like an ellipsoid with three principal axes of inertia, have attracted a lot of attention in nuclear structure physics over the last years. When such a nucleus rotates, the lowest energy state for a given angular momentum  $I$  (called yrast state) corresponds to a uniform rotation about the principal axis with the largest moment of inertia (MoI). At a slightly higher excitation energy, this axis can execute a precession motion (in the form of harmonic oscillation) about the space-fixed angular momentum vector. This describes the phenomenon of the so-called wobbling motion that has been first proposed by Bohr and Mottelson in the 1970s [1]. Since this collective mode is a rotation about a principal axis, the related energy spectra come as a series of rotational  $\Delta I = 2$  bands in which the signature of the bands alternates with increasing number of oscillation quanta  $n$ . The electric quadrupole transitions with  $\Delta I = 1$  and  $n \rightarrow n - 1$  are induced by a wobbling motion of the entire charged rigid body, and thus get collectively enhanced.

Recent studies of the nuclear wobbling motion have been triggered by the novel concepts of *transverse* wobbling (TW) and *longitudinal* wobbling (LW) proposed by Frauendorf and Dönau [2]. These authors have classified

the wobbling modes in the presence of a high- $j$  quasi-particle according to the relative orientation of the angular momentum of the quasi-particle  $\mathbf{j}_p$  and the principal axis with the largest MoI, which is usually the medium axis. If this relative orientation is perpendicular, one speaks of a *transverse* wobbling mode, and the corresponding wobbling energy decreases with the spin  $I$ . It has been observed experimentally for the nuclei  $^{161}\text{Lu}$  [3],  $^{163}\text{Lu}$  [4, 5],  $^{165}\text{Lu}$  [6],  $^{167}\text{Lu}$  [7], and  $^{167}\text{Ta}$  [8] in the  $A \approx 160$  mass region, for the nuclides  $^{135}\text{Pr}$  [9, 10] and  $^{130}\text{Ba}$  [11, 12] in the  $A \approx 130$  mass region, and for the odd-neutron nuclide  $^{105}\text{Pd}$  [13] in the  $A \approx 100$  mass region. If the relative orientation is parallel, one speaks of a *longitudinal* wobbling mode, where the wobbling energy increases with the spin  $I$ . The experimental evidence for longitudinal wobbling is, however, rare and has only been reported very recently for the nuclides  $^{133}\text{La}$  [14] and  $^{187}\text{Au}$  [15].

The increase of the wobbling energy with the spin  $I$  for the nucleus  $^{133}\text{La}$  is quite unexpected, because the wobbling mode is based on the configuration  $\pi(1h_{11/2})^1$  with an orientation of the  $h_{11/2}$  proton along the short axis [14]. The same  $h_{11/2}$  proton configuration applies to the isotones  $^{135}\text{Pr}$  [9, 10] and  $^{131}\text{Cs}$  [30], which both show a decrease of the wobbling energy with the spin  $I$ , and this behavior is actually a hallmark of the transverse wobbling mode. The authors of Ref. [14] have explained the unexpected increase of the wobbling energy with spin  $I$  for  $^{133}\text{La}$  as follows. Like the isotones, this nucleus is triaxially deformed and thus it features the wobbling mode. The triaxial deformation parameters  $\beta = 0.16$  and

\*Electronic address: qbchen@pku.edu.cn

†Electronic address: sfrauend@nd.edu

‡Electronic address: nkaiser@ph.tum.de

§Electronic address: meissner@hiskp.uni-bonn.de

¶Electronic address: mengj@pku.edu.cn

$\gamma = 26^\circ$  are supported by tilted axis cranking calculations and the increase of the wobbling energy with spin  $I$  is attributed to nearly equal MoIs with respect to the short ( $s$ -) axis and medium ( $m$ -) axis ( $\mathcal{J}_s \simeq \mathcal{J}_m$ ). The  $m$ -axis is no longer preferred for alignment with the collective rotor angular momentum  $\mathbf{R}$ , which has now a larger component along the  $s$ -axis. The mechanism underlying the enlarged  $\mathcal{J}_s$ -value is attributed to the gradual alignment of a pair of positive-parity ( $gd$ ) protons with the  $s$ -axis. In the calculations of Ref. [14], this mechanism is taken into account by introducing a spin-dependent MoI for  $\mathcal{J}_s$ . Such a scenario is obviously more complex than the classification scheme suggested in Ref. [2], which assumes  $\mathcal{J}_s < \mathcal{J}_m$ . Therefore, the situation in  $^{133}\text{La}$  corresponds to an intermediate coupling scheme.

Very recently, in Ref. [16] the  $g$ -factor and the static (spectroscopic) quadrupole moment (SQM) were measured for the bandhead state (an  $11/2^-$  isomeric state) of the yrast band of  $^{133}\text{La}$ . The obtained  $g$ -factor is  $g = 1.16 \pm 0.07$  and SQM is  $|Q| = 1.71 \pm 0.34$  eb. On the theoretical side, Monte Carlo shell-model (MCSM) calculations gave  $g = 1.16$  and provided the information that the dominant configuration of the  $11/2^-$  isomeric state is  $\pi(1h_{11/2})^1$ . At the same time, these calculations predicted  $Q = -1.25$  eb. The distribution of the quadrupole moment expectation values obtained with shell-model wave functions for the  $11/2^-$  state indicates a triaxial shape with deformation parameters  $\beta \sim 0.16$  and  $\gamma \sim 20^\circ$  [16], which is consistent with the wobbling interpretation. These new results motivate us to investigate the  $g$ -factor and SQM as functions of the spin  $I$  in the wobbling motion by taking the case of  $^{133}\text{La}$  as the first example.

Our calculations are carried out with the particle rotor model (PRM), which has been used widely for describing wobbling bands and has achieved much success in this respect [2, 4, 5, 10, 12–15, 17–21]. In Ref. [14], the PRM (there called “quasi-particle plus triaxial rotor model”) could reproduce well the experimental energy spectra and wobbling energies together with the electromagnetic transition probability ratios  $B(M1)_{\text{out}}/B(E2)_{\text{in}}$  and  $B(E2)_{\text{out}}/B(E2)_{\text{in}}$  for the wobbling bands in  $^{133}\text{La}$ . In this work we use the same triaxial deformation parameters  $\beta = 0.16$  and  $\gamma = 266^\circ$  as in Ref. [14]. With this chosen value of  $\gamma$ , the 1-axis, 2-axis, and 3-axis are the conventional  $s$ -axis,  $l$ -axis, and  $m$ -axis of the triaxially deformed ellipsoid, respectively. The MoIs of the nuclear core are taken as  $\mathcal{J}_m = 15.33 \text{ } \hbar^2/\text{MeV}$ ,  $\mathcal{J}_l = 2.92 \text{ } \hbar^2/\text{MeV}$ , and  $\mathcal{J}_s = [9.125 + 0.657(I - j)] \text{ } \hbar^2/\text{MeV}$  for the  $m$ -,  $l$ -, and  $s$ -axes, respectively [14]. Here,  $I$  and  $j = 11/2$  are the quantum numbers related to the total angular momentum  $\mathbf{I}$  and the proton angular momentum  $\mathbf{j}_p$ .

In the following, the methods to calculate the  $g$ -factor and SQM are given. For an odd-mass nuclear system the rotor angular momentum  $\mathbf{R}$  and the (proton) particle angular momentum  $\mathbf{j}_p$  are coupled to the total spin  $\mathbf{I}$  as

$$\mathbf{R} + \mathbf{j}_p = \mathbf{I}. \quad (1)$$

The magnetic moment  $\mu$  of this system is calculated from the (rotational) wave function  $|I, M = I\rangle$ , with  $M$  the quantum number related to the projection of  $\mathbf{I}$  onto the  $z$ -axis of the laboratory frame, as follows

$$\mu = gI = \langle II | g\hat{I}_z | II \rangle = \langle II | g_p \hat{j}_{pz} + g_R \hat{R}_z | II \rangle, \quad (2)$$

where  $\hat{I}_z$ ,  $\hat{j}_{pz}$ , and  $\hat{R}_z$  are the  $z$ -components of the respective angular momentum operators. Moreover,  $g_p$  and  $g_R$  are the gyromagnetic ratios of the proton-particle and the core, while the output quantity  $g$  refers to the total nuclear system. In the present study, we use the values  $g_R = Z/A = 0.43$  for the rotor and  $g_p = 1.21$  for the  $h_{11/2}$  valence-proton, in which the spin  $g$ -factor  $g_s = 3.35$  has been reduced to 0.6 times that of a free proton [1]. The possible modification of  $g_R$  by the ( $dg$ ) quasi-proton alignment can be neglected, because the spin contribution to the  $g$ -factor is small for normal-parity single-particle states.

By using the generalized Landé formula, the matrix element in Eq. (2) can be expressed through scalar products of angular momentum operators as

$$\mu = \frac{\langle II | g_p \mathbf{j}_p \cdot \mathbf{I} + g_R \mathbf{R} \cdot \mathbf{I} | II \rangle}{I(I+1)} \langle II | \hat{I}_z | II \rangle. \quad (3)$$

After some rearrangement of terms, the  $g$ -factor of the total nuclear system is given by

$$g = \frac{\langle g_p \mathbf{j}_p \cdot \mathbf{I} + g_R \mathbf{R} \cdot \mathbf{I} \rangle}{I(I+1)} \quad (4)$$

$$= g_R + (g_p - g_R) \frac{\langle \mathbf{j}_p \cdot \mathbf{I} \rangle}{I(I+1)} \quad (5)$$

$$= g_R + (g_p - g_R) \frac{j(j+1)}{I(I+1)} + (g_p - g_R) \frac{\langle \mathbf{j}_p \cdot \mathbf{R} \rangle}{I(I+1)} \quad (6)$$

$$= \frac{1}{2} \left[ (g_p + g_R) + (g_p - g_R) \frac{j(j+1) - \langle \mathbf{R}^2 \rangle}{I(I+1)} \right]. \quad (7)$$

From Eqs. (5) and (6), one sees that the  $g$ -factor reflects the relative orientations between  $\mathbf{j}_p$ ,  $\mathbf{R}$ , and  $\mathbf{I}$ . In particular, one gets  $g = g_R$  in the case  $\mathbf{j}_p \perp \mathbf{I}$ , while

$$g = g_R + (g_p - g_R) \sqrt{\frac{j(j+1)}{I(I+1)}} \quad (8)$$

in the case  $\mathbf{j}_p \parallel \mathbf{I}$ , and

$$g = g_R + (g_p - g_R) \frac{j(j+1)}{I(I+1)} \quad (9)$$

in the case  $\mathbf{j}_p \perp \mathbf{R}$ . It is worth mentioning here that the  $g$ -factor has been used to investigate the angular momentum coupling scheme in chiral doublet bands [22, 23]. According to Eq. (7), one can get from the resulting  $g$ -factor also information about the rotor angular momentum, via the expectation value  $\langle \mathbf{R}^2 \rangle$ .

The SQM gives a measure of the nuclear charge distribution associated with the collective rotational motion, and it is calculated as [1, 24]

$$Q(I) = \langle II | \hat{Q}_{20} | II \rangle, \quad (10)$$

where the quadrupole moment operator in the laboratory frame  $\hat{Q}_{20}$  is obtained from the intrinsic quadrupole moments  $Q'_{2\nu}$  by multiplication with Wigner D-functions:

$$\hat{Q}_{20} = \sum_{\nu} D_{0,\nu}^2 Q'_{2\nu}. \quad (11)$$

The 5 intrinsic quadrupole moments are  $Q'_{20} = Q'_0 \cos \gamma$ ,  $Q'_{21} = Q'_{2-1} = 0$ ,  $Q'_{22} = Q'_{2-2} = Q'_0 \sin \gamma / \sqrt{2}$ , where  $Q'_0$  is an empirical quadrupole moment that is related to the axial deformation  $\beta$  by  $Q'_0 = 3R_0^2 Z \beta / \sqrt{5\pi}$ , with  $Z$  the proton number and  $R_0 = 1.2 \text{ fm } A^{1/3}$ .

In Ref. [25], it is shown that the SQM can be also calculated from expectation values of the squared total angular momentum components along the three principal axes  $\langle \hat{I}_k^2 \rangle$  as

$$Q(I) = Q_0(I) + Q_2(I), \quad (12)$$

$$Q_0(I) = \frac{3\langle \hat{I}_3^2 \rangle - I(I+1)}{(I+1)(2I+3)} Q'_0 \cos \gamma, \quad (13)$$

$$Q_2(I) = \frac{\sqrt{3}(\langle \hat{I}_1^2 \rangle - \langle \hat{I}_2^2 \rangle)}{(I+1)(2I+3)} Q'_0 \sin \gamma. \quad (14)$$

Therefore, the SQM can provide information about the orientation of the total nuclear system relative to the principal axes frame. Note that in the prolate case  $\gamma = 0^\circ$ , when  $\langle \hat{I}_3 \rangle = K$  is a good quantum number, the part  $Q_2(I)$  vanishes and  $Q(I)$  becomes

$$Q(I) = \frac{3K^2 - I(I+1)}{(I+1)(2I+3)} Q'_0. \quad (15)$$

Using this formula, a deformation parameter of  $\beta = 0.28 \pm 0.10$  has been extracted in Ref. [16] under the assumption  $K = 1/2$  from the measured SQM  $|Q| = 1.71 \pm 0.34 \text{ eb}$  for the  $11/2^-$  isomeric state at the bandhead of  $^{133}\text{La}$ .

In Fig. 1, we show the  $g$ -factors and SQMs as functions of the spin  $I$  as calculated in the PRM for states in the yrast and wobbling bands of  $^{133}\text{La}$  in comparison with the available experimental data [16].

The PRM reproduces well the experimental  $g$ -factor at the bandhead of the yrast band. The theoretical prediction  $g = 1.16$  is in excellent agreement with the experimental value  $g = 1.16 \pm 0.07$ . The calculated  $g$ -factors decrease with increasing spin  $I$ . This feature comes mainly from the denominator  $I(I+1)$  in Eqs. (5)–(7). Over the entire spin region the  $g$ -factors for states in the yrast band are larger than those for states in the wobbling band. According to Eq. (7), this suggests that the rotor angular momentum  $R$  is smaller in the yrast band than in the wobbling band, since  $g_p - g_R = 0.78$  is positive. In the following, we will see that this behavior is induced by a wobbling motion.

In Fig. 1(a), we also show the  $g$ -factors as functions of  $I$  for the special cases  $\mathbf{j}_p \perp \mathbf{I}$ ,  $\mathbf{j}_p \parallel \mathbf{I}$ , and  $\mathbf{j}_p \perp \mathbf{R}$ . One can observe that for  $\mathbf{j}_p \parallel \mathbf{I}$  the  $g$ -factor is quite close the results obtained in the yrast and wobbling bands,

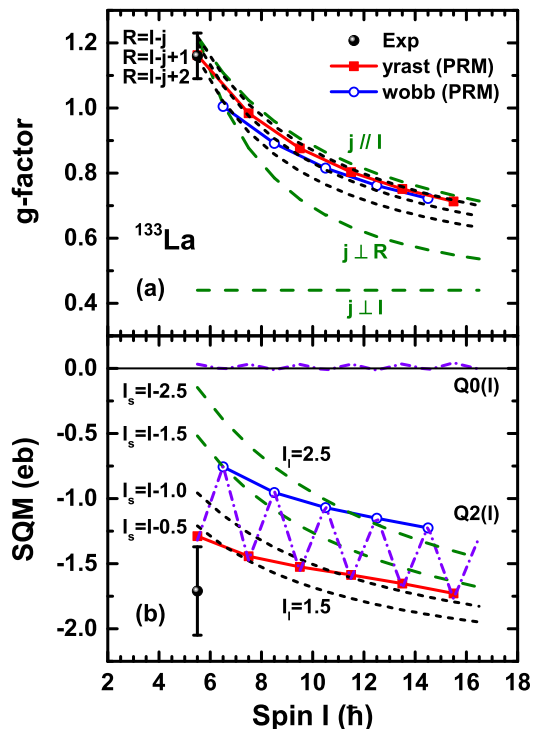


FIG. 1:  $g$ -factors (a) and static quadrupole moments (b) as functions of the spin  $I$  calculated in the PRM for the yrast and wobbling bands in  $^{133}\text{La}$  in comparison to the available data [16]. (a) The dashed lines correspond to parallel and perpendicular couplings of the angular momenta of the proton and rotor. The short dashed lines represent the formula in Eq. (7) evaluated with different rotor angular momentum quantum numbers:  $R = I - j$ ,  $I - j + 1$ , and  $I - j + 2$ . (b) The dashed-dot lines for  $Q_0(I)$  and  $Q_2(I)$  follow from Eqs. (13) and (14). The dashed and short-dashed lines show  $Q_2(I)$  calculated by Eq. (14) using the values of  $I_s$  and  $I_l$  as specified in the figure.

whereas in the other two cases it lies far away. This indicates the angular momenta of the proton  $\mathbf{j}_p$  and total nuclear system  $\mathbf{I}$  are oriented almost parallel to each other in the yrast and wobbling bands. For illustration we present also the  $g$ -factor according to Eq. (7), with  $\langle \mathbf{R}^2 \rangle = R(R+1)$  taking rotor angular momentum quantum numbers:  $R = I - j$ ,  $R = I - j + 1$ , and  $R = I - j + 2$ . One sees that the curve with  $R = I - j + 2$  agrees best with the experimental values at  $I = 11/2$ , which indicates that the rotor angular momentum quantum number  $R$  is close to  $R = 2$  at the bandhead. For higher spins  $I$  the curves  $R = I - j$  and  $R = I - j + 1$  agree better with experimental values in the yrast and wobbling bands, respectively.

At  $I = 11/2$  the calculated SQM  $Q(11/2) = -1.29 \text{ eb}$  comes out close to upper limit of the experimental value  $Q(11/2) = -1.71 \pm 0.34 \text{ eb}$ . We note that the more sophisticated MCSM calculations in Ref. [16] give  $Q(11/2) = -1.25 \text{ eb}$ . This good agreement indicates that calculations in the PRM have correctly accounted for the

structure of the collective (rotational) states. The calculated SQM decreases with increasing spin  $I$  as a consequence of the denominator  $(I+1)(2I+3)$  in Eqs. (13)-(14).

In Fig. 1(b) results for the contributions  $Q_0(I)$  and  $Q_2(I)$  as calculated by Eqs. (13) and (14) are shown separately. It is found that  $Q_0(I)$  is almost zero, since it gets strongly suppressed by the factor  $\cos\gamma = -0.07$ . Hence,  $Q_2(I) \simeq Q(I)$  which is shown in the lower part of Fig. 1(b) for the following values of total angular components along the  $s$ -axis and  $l$ -axis:  $(I_s, I_l) = (I-1/2, 3/2)$ ,  $(I-1, 3/2)$ ,  $(I-3/2, 5/2)$ , and  $(I-5/2, 5/2)$ . The former two and latter two curves agree with the experimental results for states in the yrast and wobbling bands, respectively. Clearly, the  $I_s$  values in the yrast band are larger than those in the wobbling band. We shall see that this feature is again caused by the wobbling motion. Altogether, the values  $Q_2(I) \simeq Q(I)$  are smaller for states in the yrast band than in the wobbling band (note that  $\sin\gamma = -0.99$ ). At the same time, the negative values of the SQMs are caused by the fact that the total angular momentum  $\mathbf{I}$  aligns mainly along the  $s$ -axis.

In order to better understand the behavior of the  $g$ -factor and SQM as functions of the spin  $I$ , we will discuss in the following the angular momentum geometry of the proton-particle and the collective rotor.

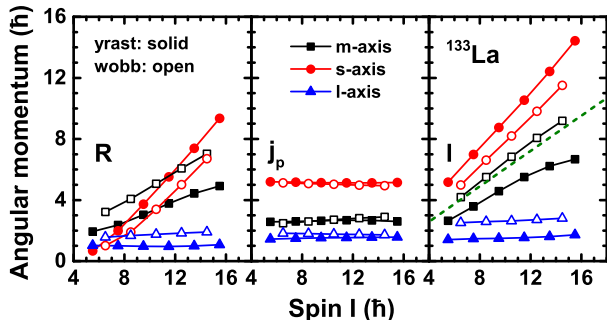


FIG. 2: Angular momentum components along the intermediate ( $m$ -), short ( $s$ -), and long ( $l$ -) axis of the rotor ( $\mathbf{R}$ ), proton-particle ( $\mathbf{j}_p$ ), and total nuclear system ( $\mathbf{I}$ ) as functions of the spin  $I$  for the yrast and wobbling bands in  $^{133}\text{La}$ . Each component is a root-mean-square expectation value of an angular momentum operator, e.g.  $I_s = \langle \hat{I}_s^2 \rangle^{1/2}$ . The dashed lines corresponds to the average quantity  $\sqrt{I(I+1)}/3$ .

In Fig. 2, we present the calculated angular momentum components along the  $m$ -,  $s$ -, and  $l$ -axis of the rotor ( $\mathbf{R}$ ), proton-particle ( $\mathbf{j}_p$ ), and total nuclear system ( $\mathbf{I}$ ) as functions of the spin  $I$  for the yrast and wobbling bands in  $^{133}\text{La}$ . The proton angular momentum  $\mathbf{j}_p$  aligns mainly with the  $s$ -axis, because its torus-like probability distribution has a maximal overlap with the triaxial nuclear core in the  $ml$ -plane [26]. The  $s$ -component is constant  $j_s \simeq 5$  over the whole spin region for both the yrast and the wobbling band. The  $\mathbf{R}$  favors an alignment in the  $sm$ -plane with a very small  $l$ -component, because  $\mathcal{J}_l$  is the

smallest. With increasing spin  $I$ , the  $R_s$  increases faster than  $R_m$ , due to the gradually increase of  $\mathcal{J}_s$ . This behavior of  $\mathbf{R}$  combined with  $\mathbf{j}_p$  gives that  $I_s$  is the largest. The latter feature leads to the negative values of  $Q_2(I)$  as shown in Fig. 1(b). In addition, the component  $I_s$  ( $I_m$ ) for states in the yrast band is larger (smaller) than for those in the wobbling band. A wobbling motion takes place about the  $s$ -axis, as it also occurs in the neighboring isotone  $^{135}\text{Pr}$  [9, 10]. The additional alignment of  $R_s$ , due to the increase of  $\mathcal{J}_s$ , stabilizes the wobbling motion about  $s$ -axis. This fact is consistent with increasing wobbling energies [14]. Since  $\mathcal{J}_s$  and  $\mathcal{J}_m$  are almost equal, a classification of the wobbling mode as longitudinal or transverse seems inappropriate. The angular momentum geometry is just more complex, corresponding to an intermediate situation between the two limits.

Moreover, the component  $I_m$  is close to the average quantity  $\sqrt{I(I+1)}/3$ . This explains why the contribution  $Q_0(I)$  almost vanishes, as shown in Fig. 1(b). The component  $I_l$  is small, with a value  $I_l \approx 3/2$  for the yrast band and  $I_l \approx 5/2$  for the wobbling band. This explains why the outcome of the analytical formula for  $Q_2(I)$  in Eq.(14) agrees so well with the full calculation in the PRM for yrast and wobbling bands.

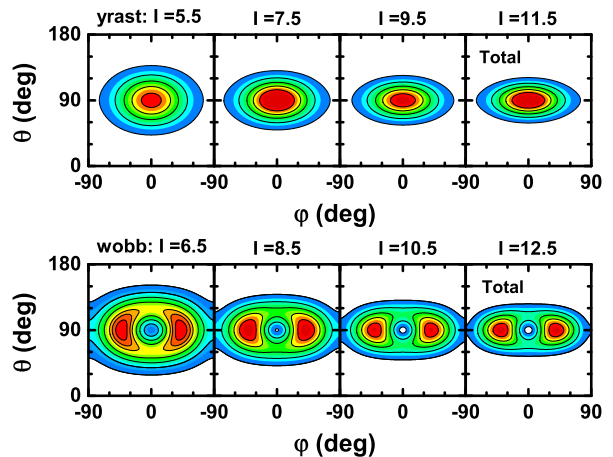


FIG. 3: Azimuthal plots, i.e., probability density distributions for the orientation of the angular momentum  $\mathbf{I}$  on the  $\theta\varphi$ -sphere as calculated in the PRM for states in the yrast and wobbling bands of  $^{133}\text{La}$ .

In order to illustrate further the wobbling motion about the  $s$ -axis, the probability density distributions  $\mathcal{P}(\theta, \varphi)$  for the orientation of the total angular momentum  $\mathbf{I}$  on the  $\theta\varphi$ -sphere (called azimuthal plots [20, 27–29]) are shown in Fig. 3 for states in the yrast and wobbling bands of  $^{133}\text{La}$ . Here,  $\theta$  is a polar angle between the total spin  $\mathbf{I}$  and the  $l$ -axis, and  $\varphi$  is an azimuthal angle in the  $sm$ -plane measured from the  $s$ -axis. Over the entire spin region, the distributions  $\mathcal{P}(\theta, \varphi)$  are centered about  $\theta = 90^\circ$ , which corresponds to very small  $I_l$ -components, as shown earlier in Fig. 2. For states in the yrast band the maximum lies at  $\varphi = 0^\circ$ , which represents a highest



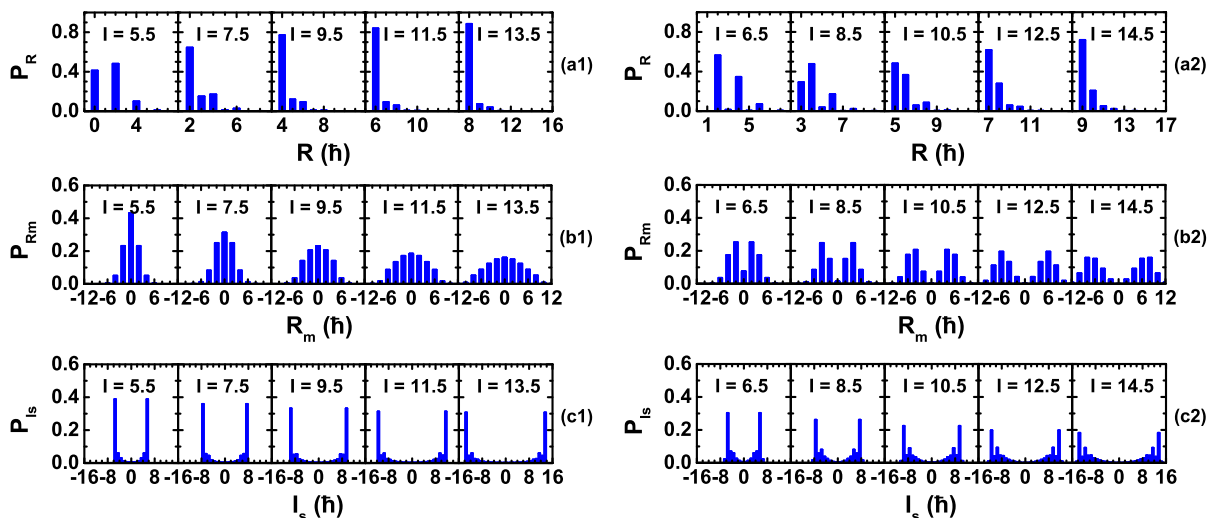


FIG. 4: Probability distributions for the rotor angular momentum ( $R$ -plot  $P_R$ , a1-a2), for the projection of the rotor angular momentum onto the  $m$ -axis ( $K_R$ -plot  $P_{R_m}$ , b1-b2), and for the projection of the total angular momentum onto the  $s$ -axis ( $K$ -plot  $P_{I_s}$ , c1-c2) as calculated in the PRM for states in the yrast and wobbling bands of  $^{133}\text{La}$ .

probability of aligning  $\mathbf{I}$  along the  $s$ -axis. To the contrary, states in the wobbling band have a minimum at  $\varphi = 0$ . For these wobbling states, the maximal probability lies on a rim around the minimum, and  $\mathcal{P}(\theta, \varphi)$  reflects in this way the wobbling motion (or precession) of  $\mathbf{I}$  about the  $s$ -axis. Note that one obtains here precisely the distributions as expected for the wobbling motion [12, 20], namely  $\varphi$ -symmetric wave functions for the ( $n = 0$ ) yrast band and  $\varphi$ -antisymmetric wave functions for the ( $n = 1$ ) wobbling band. Moreover, the feature that the distributions centered at  $\varphi = 0^\circ$  do not extend out to  $\varphi = \pm 90^\circ$  indicates that the wobbling mode in  $^{133}\text{La}$  is very stable, which is guaranteed by a gradual increase of  $\mathcal{J}_s$  with  $I$ .

In Fig. 4, we show the calculated probability distributions for the rotor angular momentum ( $R$ -plots  $P_R$ , a1-a2), for the projection of the rotor angular momentum onto the  $m$ -axis ( $K_R$ -plots  $P_{R_m}$ , b1-b2), and for the projection of the total angular momentum onto the  $s$ -axis ( $K$ -plots  $P_{I_s}$ , c1-c2) in the yrast and wobbling bands of  $^{133}\text{La}$ . These detailed results do further support the picture of a wobbling motion about the  $s$ -axis.

The  $R$ -plots (a1) and (a2) show a similar behavior as those for the nucleus  $^{135}\text{Pr}$  [20], namely, for states in the yrast band  $R$  is almost a good quantum number. The  $P_R$ -distributions have a pronounced peak at the minimum value of  $R = I - j$ , except for the bandhead with  $I = 11/2$ , where the maximal weight occurs at  $R = I - j + 2 = 2$ . For states in the wobbling band an admixture of substates with  $R = I - j$  and  $R = I - j + 1$  is present. An exception occurs again at the bandhead  $I = 13/2$ , where the peaks lie at  $R = I - j + 1$  and  $I - j + 3$ . According to these characteristics, one can understand the behavior of the  $g$ -factor as a function of spin  $I$ , as shown in Fig. 1(a).

The  $K_R$ -plots (b1) and (b2) illustrate how the picture

of a wobbling oscillation arises. The distributions  $P_{R_m}$  display large admixtures of various values of  $R_m$ , which have their origin in the wobbling motion of the rotor towards to the  $m$ -axis. At  $R_m = 0$ , the distribution  $P_{R_m}$  has a finite value for states in the yrast band, while it vanishes for states in the wobbling band. This is a characteristic of the one-phonon excitation of the wobbling mode and it is consistent with the  $\varphi$ -symmetric wave functions for ( $n = 0$ ) yrast states and  $\varphi$ -antisymmetric wave functions for ( $n = 1$ ) wobbling states, as visualized by the azimuthal plots  $\mathcal{P}(\theta, \varphi)$  in Fig. 3.

The  $K$ -plots (c1) and (c2) display that the prominent peaks of the distribution  $P_{I_s}$  appear at  $I_s = \pm I$  for states in the yrast band and at  $I_s = \pm(I - 1)$  for states in the wobbling band. This corresponds to the classical picture of the wobbling motion. The yrast state with spin  $I$  and the neighboring wobbling state with spin  $I + 1$  have similar angular momentum components along the  $s$ -axis. The total angular momentum in a wobbling state with  $I + 1$  has to precess (wobble) with respect to  $s$ -axis to reach  $I_s \simeq I$ .

In summary, the  $g$ -factor and SQM for the wobbling mode of  $^{133}\text{La}$  have been investigated in the framework of the PRM. The calculation reproduces the available  $g$ -factor and SQM data well. The properties of the  $g$ -factor and SQM as functions of spin  $I$  have been interpreted by analyzing the angular momentum components of the rotor, proton-particle, and total nuclear system with the help of various quantum mechanical probability distributions: Azimuthal plots,  $R$ -plots,  $K_R$ -plots, and  $K$ -plots. It has been demonstrated that the wobbling mode in  $^{133}\text{La}$  corresponds to a wobbling of  $\mathbf{I}$  about the  $s$ -axis. The  $g$ -factor at the bandhead of yrast band gives the information  $R \simeq 2$  about the rotor angular momentum  $\mathbf{R}$ . The variation of the  $g$ -factor with spin  $I$  indicates that

the angular momenta of the proton-particle and total nuclear system are oriented parallel to each other. The negative values of SQMs are caused by the fact that the total angular momentum  $I$  aligns with the  $s$ -axis. The differences of the SQM between states in the yrast and wobbling bands can be traced back to the wobbling motion. Therefore, the  $g$ -factor and SQM are good probes for depicting the picture of wobbling motion. Future experimental measurements of  $g$ -factors and the SQMs for states in the high-spin region are strongly suggested in order to test the theoretical predictions presented in this work.

### Acknowledgements

This work has been supported in parts by Deutsche Forschungsgemeinschaft (DFG) and National Natural

Science Foundation of China (NSFC) through funds provided by the Sino-German CRC 110 “Symmetries and the Emergence of Structure in QCD” (DFG Grant No. TRR110 and NSFC Grant No. 11621131001), the US Department of Energy (Grant No. DE-FG02-95ER40934), the National Key R&D Program of China (Contract No. 2017YFE0116700 and No. 2018YFA0404400), the NSFC under Grant No. 11935003, and the State Key Laboratory of Nuclear Physics and Technology of Peking University (Grant No. NPT2020ZZ01). The work of U.-G.M. was also supported by the Chinese Academy of Sciences (CAS) through a President’s International Fellowship Initiative (PIFI) (Grant No. 2018DM0034) and by the VolkswagenStiftung (Grant No. 93562).

- 
- [1] A. Bohr and B. R. Mottelson, *Nuclear structure*, vol. II (Benjamin, New York, 1975).
- [2] S. Frauendorf and F. Dönau, *Phys. Rev. C* **89**, 014322 (2014).
- [3] P. Bringel, G. B. Hagemann, H. Hübel, A. Al-khatib, P. Bednarczyk, A. Bürger, D. Curien, G. Gangopadhyay, B. Herskind, D. R. Jensen, et al., *Eur. Phys. J. A* **24**, 167 (2005).
- [4] S. W. Ødegård, G. B. Hagemann, D. R. Jensen, M. Bergström, B. Herskind, G. Sletten, S. Törmänen, J. N. Wilson, P. O. Tjøm, I. Hamamoto, et al., *Phys. Rev. Lett.* **86**, 5866 (2001).
- [5] D. R. Jensen, G. B. Hagemann, I. Hamamoto, S. W. Ødegård, B. Herskind, G. Sletten, J. N. Wilson, K. Spohr, H. Hübel, P. Bringel, et al., *Phys. Rev. Lett.* **89**, 142503 (2002).
- [6] G. Schönwaßer, H. Hübel, G. B. Hagemann, P. Bednarczyk, G. Benzoni, A. Bracco, P. Bringel, R. Chapman, D. Curien, J. Domscheit, et al., *Phys. Lett. B* **552**, 9 (2003).
- [7] H. Amro, W. C. Ma, G. B. Hagemann, R. M. Diamond, J. Domscheit, P. Fallon, A. Gorgen, B. Herskind, H. Hübel, D. R. Jensen, et al., *Phys. Lett. B* **553**, 197 (2003).
- [8] D. J. Hartley, R. V. F. Janssens, L. L. Riedinger, M. A. Riley, A. Aguilar, M. P. Carpenter, C. J. Chiara, P. Chowdhury, I. G. Darby, U. Garg, et al., *Phys. Rev. C* **80**, 041304(R) (2009).
- [9] J. T. Matta, U. Garg, W. Li, S. Frauendorf, A. D. Ayangeakaa, D. Patel, K. W. Schlx, R. Palit, S. Saha, J. Sethi, et al., *Phys. Rev. Lett.* **114**, 082501 (2015).
- [10] N. Sensharma, U. Garg, S. Zhu, A. D. Ayangeakaa, S. Frauendorf, W. Li, G. Bhat, J. A. Sheikh, M. P. Carpenter, Q. B. Chen, et al., *Phys. Lett. B* **792**, 170 (2019).
- [11] C. M. Petrache, P. M. Walker, S. Guo, Q. B. Chen, S. Frauendorf, Y. X. Liu, R. A. Wyss, D. Mengoni, Y. H. Qiang, A. Astier, et al., *Phys. Lett. B* **795**, 241 (2019).
- [12] Q. B. Chen, S. Frauendorf, and C. M. Petrache, *Phys. Rev. C* **100**, 061301(R) (2019).
- [13] J. Timár, Q. B. Chen, B. Kruzsic, D. Sohler, I. Kuti, S. Q. Zhang, J. Meng, P. Joshi, R. Wadsworth, K. Starosta, et al., *Phys. Rev. Lett.* **122**, 062501 (2019).
- [14] S. Biswas, R. Palit, S. Frauendorf, U. Garg, W. Li, G. H. Bhat, J. A. Sheikh, J. Sethi, S. Saha, P. Singh, et al., *Eur. Phys. J. A* **55**, 159 (2019).
- [15] N. Sensharma, U. Garg, Q. B. Chen, S. Frauendorf, D. P. Burdette, J. L. Cozzi, K. B. Howard, S. Zhu, M. P. Carpenter, P. Copp, et al., *Phys. Rev. Lett.* **124**, 052501 (2020).
- [16] M. S. R. Laskar, R. Palit, S. N. Mishra, N. Shimizu, Y. Utsuno, E. Ideguchi, U. Garg, S. Biswas, F. S. Babra, R. Gala, et al., *Phys. Rev. C* **101**, 034315 (2020).
- [17] I. Hamamoto, *Phys. Rev. C* **65**, 044305 (2002).
- [18] I. Hamamoto and B. R. Mottelson, *Phys. Rev. C* **68**, 034312 (2003).
- [19] W. X. Shi and Q. B. Chen, *Chin. Phys. C* **39**, 054105 (2015).
- [20] E. Streck, Q. B. Chen, N. Kaiser, and U.-G. Meißner, *Phys. Rev. C* **98**, 044314 (2018).
- [21] Q. B. Chen, N. Kaiser, U.-G. Meißner, and J. Meng, arXiv: **nucl-th**, 2003.04065 (2020).
- [22] S. Frauendorf and J. Meng, *Nucl. Phys. A* **617**, 131 (1997).
- [23] E. Grodner, J. Srebrny, C. Droste, L. Próchniak, S. G. Rohoziński, M. Kowalczyk, M. Ionescu-Bujor, C. A. Ur, K. Starosta, T. Ahn, et al., *Phys. Rev. Lett.* **120**, 022502 (2018).
- [24] P. Ring and P. Schuck, *The nuclear many body problem* (Springer Verlag, Berlin, 1980).
- [25] Q. B. Chen, N. Kaiser, U.-G. Meißner, and J. Meng, arXiv: **nucl-th**, 2005.03865 (2020).
- [26] S. Frauendorf and J. Meng, *Z. Phys. A* **356**, 263 (1996).
- [27] F. Q. Chen, Q. B. Chen, Y. A. Luo, J. Meng, and S. Q. Zhang, *Phys. Rev. C* **96**, 051303(R) (2017).
- [28] F. Q. Chen, J. Meng, and S. Q. Zhang, *Phys. Lett. B* **785**, 211 (2018).
- [29] Q. B. Chen and J. Meng, *Phys. Rev. C* **98**, 031303(R) (2018).
- [30] <http://www.nndc.bnl.gov/ensdf/>.